Structure, Vol. 9, 851–858, September, 2001, ©2001 Elsevier Science Ltd. All rights reserved. PII S0969-2216(01)00637-2

Enzyme Mechanism and Catalytic Property of β Propeller Phytase

Sejeong Shin,[1] Nam-Chul Ha,[1] Byung-Chul Oh,[2] Tae-Kwang Oh,[2] and Byung-Ha Oh[1,3]

[1] National Creative Research Initiative Center for Biomolecular Recognition
Department of Life Science and Division of Molecular and Life Science
Pohang University of Science and Technology
Pohang
Kyungbuk, 790-784
Korea

[2] Environmental Bioresources Laboratory
Korea Research Institute of Bioscience & Biotechnology
P.O. Box 115
Yusong
Taejon, 305-600
Korea

Summary

Background: Phytases hydrolyze phytic acid (*myo*-inositol-hexakisphosphate) to less-phosphorylated *myo*-inositol derivatives and inorganic phosphate. Phytases are used in animal feed to reduce phosphate pollution in the environment. Recently, a thermostable, calcium-dependent *Bacillus* phytase was identified that represents the first example of the β propeller fold exhibiting phosphatase activity. We sought to delineate the catalytic mechanism and property of this enzyme.

Results: The crystal structure of the enzyme in complex with inorganic phosphate reveals that two phosphates and four calcium ions are tightly bound at the active site. Mutation of the residues involved in the calcium chelation results in severe defects in the enzyme's activity. One phosphate ion, chelating all of the four calcium ions, is close to a water molecule bridging two of the bound calcium ions. Fluoride ion, which is expected to replace this water molecule, is an uncompetitive inhibitor of the enzyme. The enzyme is able to hydrolyze any of the six phosphate groups of phytate.

Conclusions: The enzyme reaction is likely to proceed through a direct attack of the metal-bridging water molecule on the phosphorous atom of a substrate and the subsequent stabilization of the pentavalent transition state by the bound calcium ions. The enzyme has two phosphate binding sites, the "cleavage site", which is responsible for the hydrolysis of a substrate, and the "affinity site", which increases the binding affinity for substrates containing adjacent phosphate groups. The existence of the two nonequivalent phosphate binding sites explains the puzzling formation of the alternately dephosphorylated *myo*-inositol triphosphates from phytate and the hydrolysis of *myo*-inositol monophosphates.

[3] Correspondence: bhoh@postech.ac.kr

Introduction

Phosphorylation and dephosphorylation reactions are two of the fundamental aspects of life. The reactions, catalyzed by numerous enzymes, are used for storing and retrieving chemical energies, metabolism, and signal transduction. Phosphatases are a group of enzymes that catalyze the hydrolysis of phosphomonoester bonds in biological systems. They differ in many ways; for example, in optimum pH, in molecular weight, and, perhaps most significantly, in which metal ion cofactor is required for catalysis. Phosphatases have been traditionally divided into alkaline, acid, and protein phosphatases [1], although many of them cannot be classified according to this simple scheme.

Alkaline phosphatases are typically dimers with ~57-kDa subunits, contain two Zn^{2+} ions and one Mg^{2+} ion per subunit, and have an optimum pH of above 8. One of the most studied alkaline phosphatases is the enzyme from *Escherichia coli* [2]. The reaction of the enzyme proceeds with the overall retention of its configuration, which suggests a double in-line nucleophilic displacement mechanism [3]. The bound zinc ions have been proposed to sufficiently lower the p*K*a of Ser102 and, subsequently, of a coordinated water molecule, allowing for each of them to attack a phosphorous atom in a two-step mechanism [2, 4].

The acid phosphatases exhibit an optimum pH of below ~7 and can be further divided into three different subclasses: low molecular weight acid phosphatases (M_r ~18,000), high molecular weight acid phosphatases (M_r ~50,000–60,000), and purple acid phosphatases, which contain an Fe-Fe or Fe-Zn center at the active site. The eukaryotic low molecular weight acid phosphatases have been shown to dephosphorylate the phosphotyrosyl group of proteins. Biochemical experiments demonstrated that they utilize a common catalytic mechanism involving the formation of a covalent thiophosphate intermediate that is subsequently hydrolyzed by an activated water molecule [5, 6]. The high molecular weight acid phosphatases, including *E. coli* periplasmic acid phosphatase and human prostatic and lysosomal acid phosphatases, contain a conserved RHGXRXP motif. The histidine residue has been proposed to serve as a nucleophile in the formation of a covalent phosphohistidine intermediate [7, 8]. To explain the low optimum pH of prostatic acid phosphatase [7], it has been proposed that the catalytic histidine is not protonated at low pH due to a large number of positively charged groups surrounding the residue, but nearby Asp258 is protonated and serves as a proton donor to the oxygen atom of the scissile P-O bond [8, 9].

Purple acid phosphatases, also known as "tartrate-resistant" acid phosphatases, include enzymes from beef spleen and pig allantoic fluid and contain an active Fe(II)-Fe(III) or inactive Fe(III)-Fe(III) center, whereas di-

Key words: β propeller phytase; direct phospho-transfer; enzyme mechanism; metalloenzyme; phosphatase; crystal structure

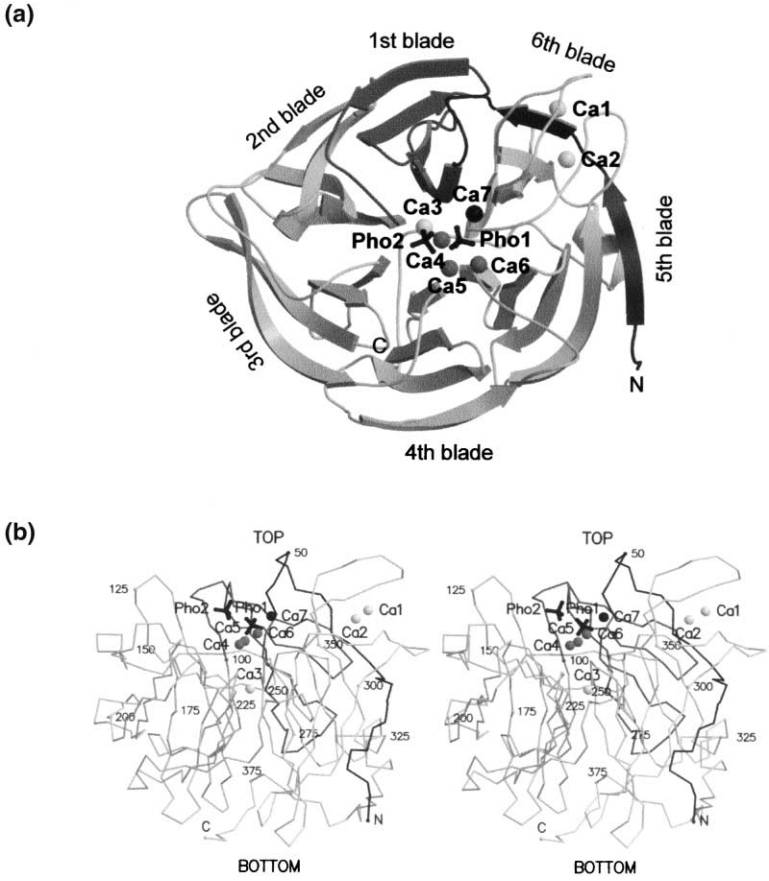

Figure 1. Overall Structure and Binding of Phosphate and Calcium Ions

(a) A ribbon diagram of the enzyme viewed down the propeller shaft. The structure contains residues 29–381 out of a total of 383 residues. The N-terminal 28 amino acids comprise a signal sequence. Three calcium ions (Ca1, Ca2, and Ca3), which are responsible mostly for the high thermal stability of the enzyme [17] and are located remotely from the active site, are shown in light gray. Three calcium ions (Ca4, Ca5, and Ca6), located at the top of the molecule, are shown in darker gray. An additional calcium ion (Ca7), which is shown in black and is not present in the absence of phosphate ions, is observed near the Ca4–Ca6 sites.

(b) A stereo view of the Cα traces of the enzyme. The "top" of the molecule is defined as one end of the molecule where the active site is located. The 6th blade and the N-terminal segment are shown in darker gray. Ca3 is located in the middle of the central channel, which corresponds to the propeller shaft.

meric 111-kDa kidney bean purple acid phosphatase contains an Fe(III)-Zn(II) center at the active site [10]. A metal-bridging or Fe(III)-coordinated hydroxide ion in the metal centers of these enzymes has been suggested to attack the phosphorous atom of a substrate directly [11]. The mechanism is similarly proposed for the serine/threonine protein phosphatases [11], which are also metalloenzymes.

Phytases are different from other phosphatases in that they prefer phytic acid as a substrate. Several phytases, including fungal phytases from *Aspergillus ficuum* [12, 13] and bacterial phytase from *E. coli* [14], have been cloned and characterized. These phytases exhibit no apparent sequence similarity to each other and to other known phosphatases, except for the RHGXRXP motif conserved in the high molecular weight acid phosphatases. The histidine residue has been proposed to serve as a nucleophile in the formation of covalent phosphoenzyme intermediates [15, 16]

Recently, we determined the structure of a novel, thermostable phytase from a *Bacillus amyloliquefacience* strain [17]. It adopts a β propeller fold, which is found in a range of different proteins and exhibits a remarkable functional diversity; for example, it plays a role in the oxidation of sugars [18] and in heme binding and delivery [19], as reviewed in [20]. A search for similar folds in the PDB database DALI [21] does not reveal any of the known phosphatase structures. The catalytic activity of the enzyme is dependent on the metal ion and is maximized by >2 mM calcium ion. The fully active form of the enzyme contains six calcium ions, while the inactive form of the enzyme contains only three calcium ions due to the loss of the other three located at the top of the molecule [17], suggesting that this region is likely to be the active site.

We have deduced a convincing catalytic mechanism of this β propeller phytase (referred to as TS-Phy, denoting thermostable phytase) on the basis of the 1.8 Å resolution structure of the enzyme complexed with phosphate ions and calcium ions in conjunction with structure-based mutagenesis and biochemical experiments. In addition, the phosphate-bound structure allowed reliable modeling of the binding of phytate and less-phosphorylated substrates, which explains the unusual catalytic property of forming alternately dephosphorylated *myo*-inositol triphosphates and hydrolysis of *myo*-inositol monophosphates.

Results

Overall Structure

TS-Phy is a β propeller consisting of five 4-stranded and one 5-stranded antiparallel β sheets aligned around a pseudo six-fold symmetry axis lying on the shaft of the propeller, which is a distinct central channel filled with many ordered water molecules. This enzyme binds seven calcium ions, two of which are located at the periphery, one of which is located in the middle of the central channel, and the other four of which are located at the top of the molecule (Figure 1). Unlike most other

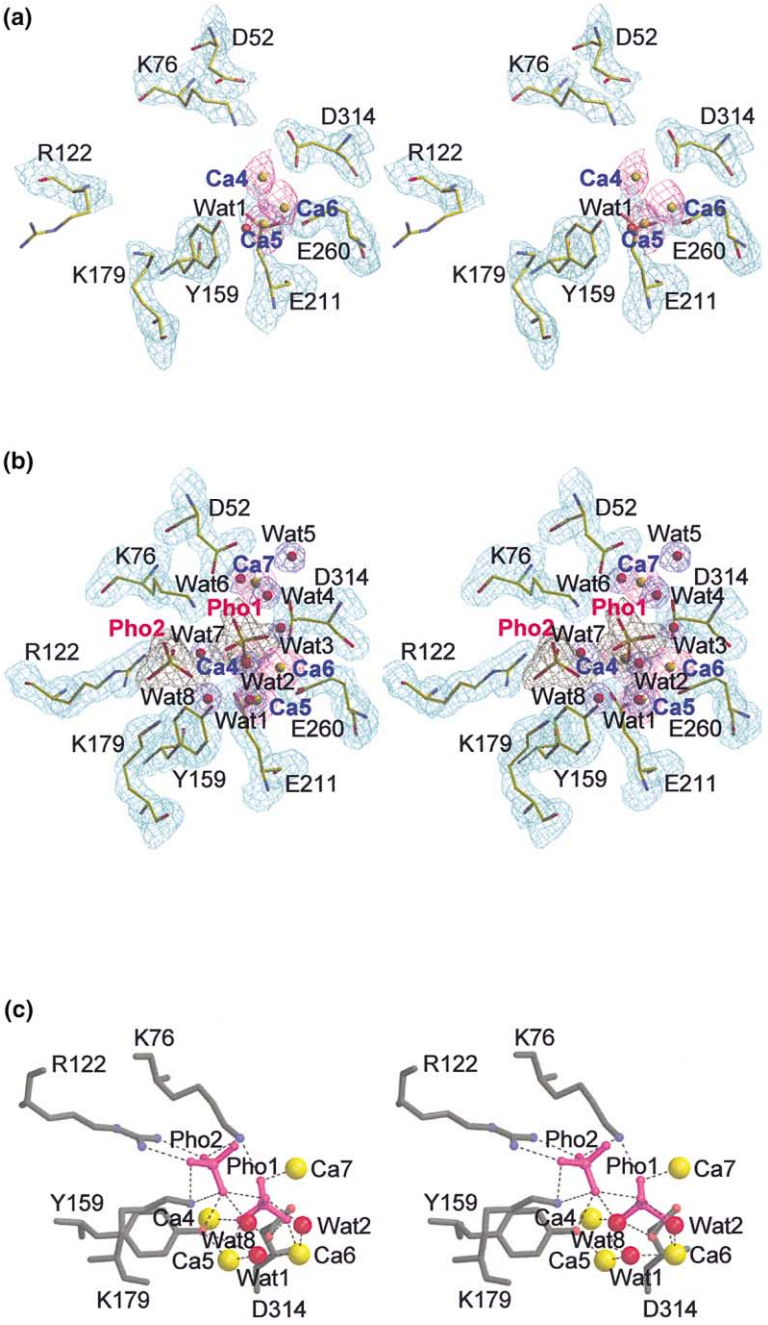

Figure 2. The Active Site of the Enzyme

(a) A stereo view of the $2F_o$-F_c electron densities (2.05 Å, contoured at 1σ) for the active site region of the phosphate-unbound structure of TS-Phy (PDB accession code: 2POO) [17]. The electron density for Wat1 is only barely visible at lower contour levels and is not apparent in this figure, nor is it included in the deposited coordinates. Other water molecules in Figure 2b do not exist in this structure.

(b) A stereo view of the $2F_o$-F_c electron densities (2.05 Å, contoured at 1σ) of the phosphate-bound structure of TS-Phy shown for the same region as in Figure 2a. The well-defined electron densities for the bound phosphate and calcium ions indicate tight bindings of these ions. Water molecules and the three positively charged residues, Lys76, Arg122, and Lys179, involved in the direct interactions with the phosphate ions are well ordered. Wat1–Wat8 correspond to residues 601–608 in the deposited coordinates.

(c) A stereo view of detailed atomic interactions of the bound phosphate ions. For clarity, not all of the nearby water molecules are shown. Figures 1 and 2 were prepared using MOLSCRIPT [30] and O [31].

β propeller structures, it does not show a conserved sequence repeat in the β strands.

Phosphate Binding to the Active Site

The enzyme binds two phosphate ions (Pho1 and Pho2) at the top of the molecule where calcium ions for triadic calcium sites (Ca4–Ca6) in the phosphate-unbound structure [17]. The phosphate ions induce binding of one more calcium ion (Ca7) by providing a coordination arm (Figure 1). The phosphate ions also induce the restructuring of a number of side chains near the binding site through hydrogen bonding and ionic interactions with these residues. The side chains of Lys76, Arg122, Tyr159, and Lys179, which are involved in the binding of phosphate ions, undergo disorder-to-order changes, as indicated by the much stronger electron densities (Figure 2a) and the lower temperature factors of these side chains compared with those in the phosphate-unbound structure. Pho1 is involved in the chelation of all of the four calcium ions. Together with the side chains of Asp52, Asp55, Tyr159, Glu211, Asp258, Glu260, Glu279, and Asp314 and seven water molecules plus the bridging water molecule (Wat1) between Ca5 and Ca6, it forms octahedral coordination shells for Ca4–Ca7 (data not shown). By these interactions, Ca4–Ca6 and the calcium-cheating water molecules exhibit very well-defined electron densities (Figure 2). In contrast, the coordination shells of Ca4–Ca6 are incomplete in the

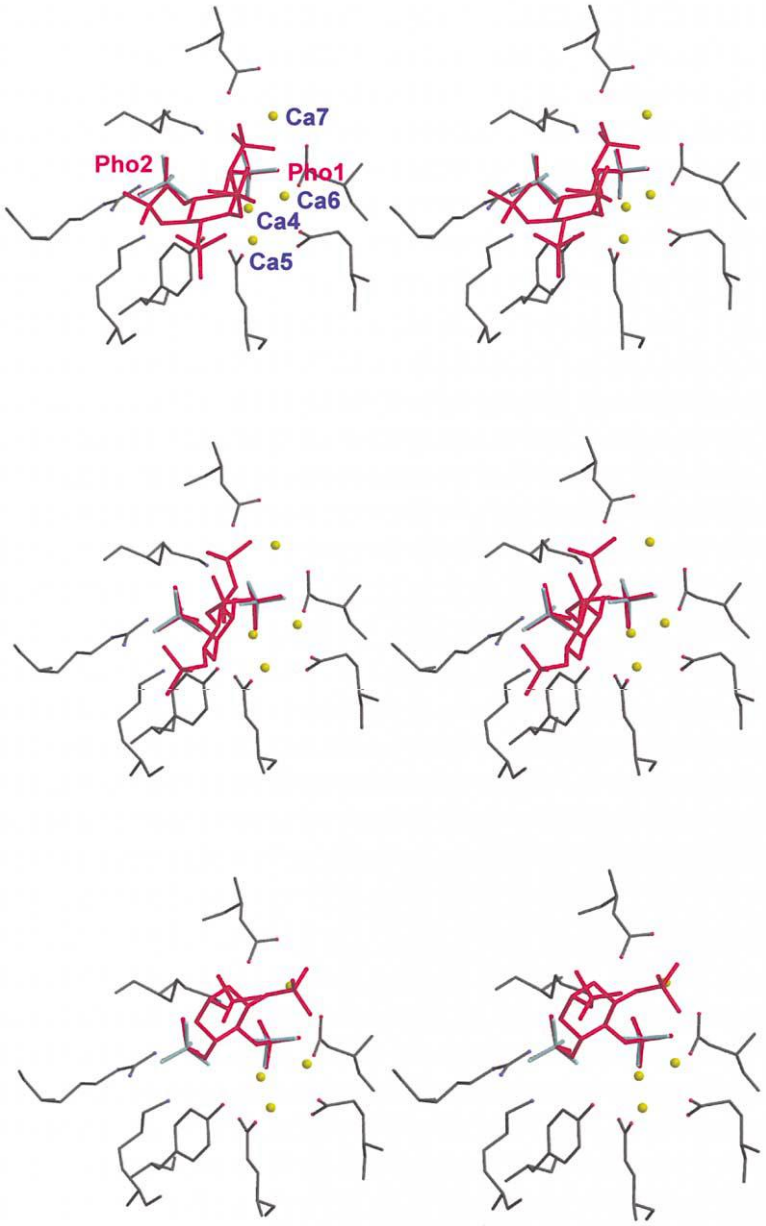

Figure 3. Model Building of Substrate Bindings

Models of phytate (top), Ins(1,2,4,5,6)P_5 (middle), and Ins(2,4,5,6)P_4 (bottom) are built at the active site. The pairs of (3-P and 4-P) of phytate, (1-P and 2-P) of Ins(1,2,4,5,6)P_5, and (5-P and 4-P) of Ins(2,4,5,6)P_4 were manually superposed on (Pho1 and Pho2), respectively. Torsion angles of the phosphate groups of the substrates were manipulated until there was no steric clash, as judged by checking the interatomic distances. Solid docking using Quanta (Molecular Simulation) showed that the bindings of the final models are energetically allowed. The substrates, bound phosphates, and calcium ions are in red, sky-blue, and yellow, respectively. The bound water molecules are omitted for clarity.

phosphate-unbound structure, and the bound water molecules including Wat1 are not, or barely, visible [17]. Pho2 does not chelate any of the calcium ions. It instead interacts directly with Lys76, Arg122, Tyr159, Lys179, and Pho1.

Hydrolysis of Ins(2)P_1 by TS-Phy

Among the phosphate groups on phytate, only the C2-phosphate is axially bonded. Notably, TS-Phy is able to cleave the phosphate group at the C2 position, while all the other known phytases are not [22]. This can be shown by the release of a phosphate ion from the enzyme reaction with *myo*-inositol 2-monophosphate (Ins[2]P_1) (data not shown). A steady-state kinetic analysis showed that the apparent K_M value of the enzyme for Ins(2)P_1 is 4.3 mM, which is 9.6 times higher than that (0.45 mM) for phytate. The apparent k_{cat} value of the enzyme for Ins(2)P_1 is 6.99 min^{-1}, which is 159 times lower than that for phytate (1110 min^{-1}). Consistently, the liberation of phosphate from Ins(2)P_1 is 680-fold slower than the liberation from phytate at the same concentrations of the substrates (2 mM). Similar enzyme assays showed that TS-Phy is also able to hydrolyze Ins(1)P_1 and Ins(4)P_1 at rates similar to the rate of Ins(2)P_1 hydrolysis (data not shown). Though not tested, the enzyme should be able to hydrolyze the other three InsP_1s (commercially unavailable), since the enzyme cleaves the phosphate group at any position on phytate, as described below.

Modeling of the Substrate Binding

Possible modes of binding of phytate and less-phosphorylated *myo*-inositols to the active site were investigated on the basis of the superposition of phosphate

groups of phytate on the two bound phosphate ions (representative binding modes are shown in Figure 3). The structure of the phytate molecule bound to an *E. coli* mutant phytase (PDB accession code: 1DKQ; 2.05 Å resolution) was used without any modification. It was readily noted that any two phosphate groups that are not adjacent to each other can not be superposed on Pho1 and Pho2 simultaneously. In addition, because phytate is a large molecule and the active site cleft of the enzyme is narrow, successful superposition on (Pho1 and Pho2) without a steric clash was limited to the pairs of (3-P and 4-P) and (6-P and 1-P). The observation suggests that, initially, only the two pairs of the phosphate groups are accessible for cleavage by the enzyme. Removal of 3-P or 6-P from the phytate molecule allowed for superposition of (1-P and 2-P) or (4-P and 5-P), respectively, but not others. The further removal of phosphate groups alleviates steric restriction in the superposition.

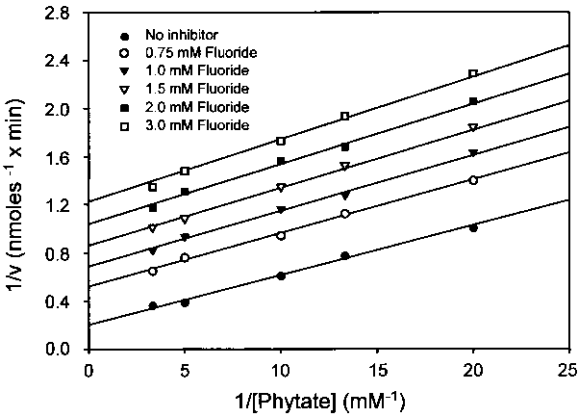

Figure 4. Inhibition by Fluoride Ion

TS-Phy at the final concentration of 2.5 μg/ml was preincubated with 1 mM $CaCl_2$ and NaF at the indicated concentrations for 5 min before it was reacted with phytate (0.05–0.3 mM) in 0.1 M Tris-HCl buffer (pH 7.0) containing 2 mM $CaCl_2$. The final volume of the reaction mixture was 5 ml. An aliquot of 0.5 ml was withdrawn every minute and assayed for the production of inorganic phosphate.

Discussion

Catalytic Mechanism

Several lines of evidence strongly suggest that Wat1 directly attacks the phosphorus atom. Firstly, since the p*K*a of a water molecule bridging two metal ions decreases significantly to a very acidic value [23], Wat1 should be a hydroxide ion, which is a reactive nucleophile. The close distance (3.7 Å) between Wat1 and the phosphorous atom of Pho1 indicates that Wat1 is suitable for initiating the catalysis on the phosphate group occupying the Pho1 site. Furthermore, the chelation of Pho1 by the four calcium ions (Figure 2b) suggests that they are suitable for neutralizing the negative charge of the pentavalent transition state generated by the proposed attack by Wat1. Consistently, the alanine substitution of Glu211 or Glu260, both of which are involved in the calcium chelation (Figure 2a), results in the complete loss of the catalytic activity [24]. Secondly, F^-, which is able to replace OH^- in binding to a protein, inhibits the enzyme activity with the apparent inhibition constant of 0.73 mM. A typical pattern of an uncompetitive inhibition was observed (Figure 4). The inhibition pattern indicates an ordered binding of the two substrates to the active site: phytate first, and then a water molecule. The structures of phytase in two different states provide a clue to how this can happen. The barely visible Wat1 in the structure of the phosphate-unbound structure indicates that the Wat1 site must have a very poor binding affinity for the hydroxide ion due to the partially disordered state of the active site in the absence of the phosphate binding as described above. Especially, Wat2 and Wat8, which are 2.94 Å and 2.62 Å apart, respectively, from Wat1 in the phosphate-bound structure, are not visible in the phosphate-unbound structure. The restructuring of the coordination shells of Ca4–Ca6 induced by the phosphate binding would convert the Wat1 site into a high-affinity site for hydroxide and fluoride ions to compete with each other for binding to. Thirdly, there is no other candidate nucleophilic group near any of the two phosphorous atoms, which may initiate the formation of a phosphoenzyme intermediate. Tyr159 is close to Pho2 (3.62 Å between the O^{η} and the phosphorous atom), but the tyrosyl oxygen is involved in the chelation of Ca5. Mutation of this residue to alanine resulted in the near loss of catalytic activity [24]. However, the defect can be attributed to the inability of the mutant to secure the binding of Ca5.

There are three possible candidates that can serve as a general acid, donating a proton to the leaving alkoxide. These are Wat2, Wat8, and the amino group of the Lys76 side chain (Figure 2b), which are 2.97, 3.45, and 4.07 Å from a Pho1 oxygen atom, respectively, which corresponds to the scissile P-O of the substrates in the modeling study. Wat2 participates in the chelation of Ca6. These water molecules and the Lys76 amino group are on a hydrogen-bonded network that includes Pho2. Therefore, regardless of which one may be a general acid in the catalysis, it is expected that the absence of the phosphate group at the Pho2 site would not secure the positions of these candidates and could result in the decrease of the catalytic efficiency. In the six calcium-loaded but phosphate-free structure of the enzyme [17], both Wat2 and Wat8 are missing, and the side chain of Lys76 is disordered. The occupation of the Pho1 site only, as in the case of the binding of an InsP_1 to it, would organize these components for the catalysis, but not to an optimal level. The indirect catalytic role of the phosphate group occupying the Pho2 site, we propose, explains the 159 times lower k_{cat} of the enzyme for Ins(2)P_1 compared with those for phytate. The proposed catalytic mechanism of the enzyme is depicted in Figure 5a. A similar and relevant description for an enzyme mechanism of a pyrophosphatase has been recently reported that includes direct in-line attack of a bi-Mg(II)-bridging water molecule and crystallographic evidence for the replacement of the activated water molecule (OH^-) by a fluoride ion that inhibits the enzyme activity [25].

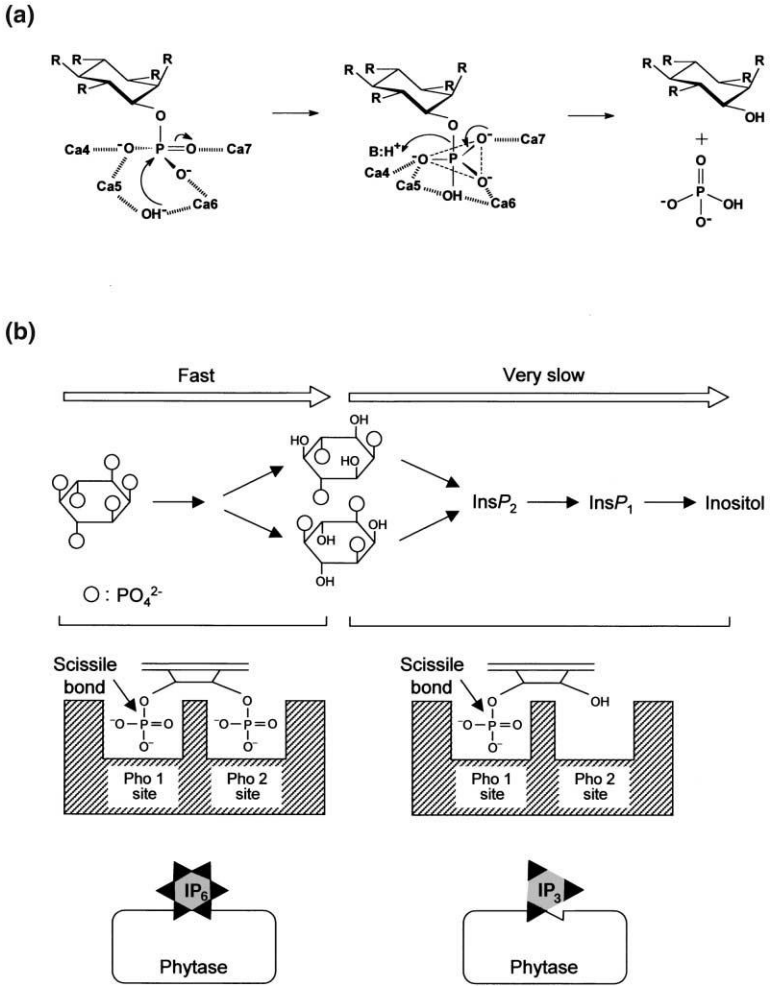

Figure 5. Proposed Enzyme Mechanism and Degradation of Phytate

(a) Enzyme mechanism. The hydroxide ion (Wat1) directly attacks the phosphorous atom of phytate occupying the Pho1 site (Figure 5b). The role of the general acid (-B:H$^+$) in the catalysis could be served by either Wat2, Wat8, or Lys76. This catalytic role appears to be severely affected in the hydrolysis of any nonadjacent phosphate group(s), where the Pho2 site is empty.

(b) The degradation of phytate consistent with the structural and biochemical data. Only two adjacent phosphate groups of the substrates can simultaneously occupy both the "cleavage site" (Pho1 site) and the "affinity site" (Pho2 site). The substrates that can occupy only the cleavage site are less favorable for binding to the enzyme and more susceptible to the inhibition by inorganic phosphate than phytate, InsP_5, and InsP_4. More critically, the indirect catalytic role of the Pho2 site, proposed in the text, is absent.

Substrate Recognition and Degradation of Phytate

A nearly identical phytase from *Bacillus subtilis* (93% sequence identity to TS-Phy) was shown to hydrolyze up to three phosphate groups from phytate [26]. The produced InsP_3s were identified as Ins(1,3,5)P_3 and Ins(2,4,6)P_3, indicating that the enzyme prefers the hydrolysis of every second phosphate over that of adjacent ones and that it can cleave any phosphate group of phytate. The production of the alternately phosphate-removed InsP_3s suggests that the enzyme preferentially recognizes the substrates containing a pair of adjacent phosphate groups over the other substrates that don't and that it cleaves one of the two bound phosphate groups. The preferential binding of phytate and the selective cleavage requires two phosphate binding sites to which two adjacent phosphate groups can bind, one of which serves as a cleavage site. This is consistent with the modeling experiment in which we found that only the phosphate groups of phytate that are adjacent to each other can be superposed onto Pho1 and Pho2 simultaneously. A phosphate group bound to the Pho1 site would be cleaved ("cleavage site"), while the other one bound to the Pho2 site increases the binding affinity ("affinity site") for the substrates containing adjacent phosphate groups (Figure 5b). This notion is supported by the 9.6-fold higher K_M value for Ins(2)P_1 than that for phytate.

In the context of the proposal, the modeling experiment explains why the phosphate groups are alternately removed during the accumulation of InsP_3s. Removal of 3-P or 6-P of phytate, which can be superposed on

Table 1. Data Collection and Refinement Statistics, F > 1σ

Resolution range (Å)	20.0–1.8
R_{sym}[a] (1.86–1.8 Å), %	5.9 (27.1)
Total reflections	250,463
Unique reflections	32,362
Completeness (1.86–1.8Å), %	94.7
R factor[b] (R_{free}[c]), %	19.7 (22.3)
Number of refined atoms	
Protein/water	2736/54
Phosphate/Ca^{2+}	2/7
Rmsd bond length deviation (Å)	0.012
Rmsd bond angle deviation (°)	1.53
Ramachandran plot (%)	
Most favored region	87.2
Additionally allowed region	12.8

[a] $R_{sym} = \Sigma\ |I_{obs} - I_{avg}|/\Sigma\ I_{obs}$.
[b] R factor $= \Sigma\ ||F_o| - |F_c||/\Sigma\ ||F_o|$, where $|F_o|$ and $|F_c|$ are the observed and calculated structure factor amplitudes, respectively.
[c] R_{free} was calculated with 5% of the data.

Pho1 without steric clash as described above, allows superposition of the other pair of phosphate groups of the resulting intermediates on (Pho1 and Pho2). For example, the removal of 3-P allows otherwise sterically prohibited binding of (1-P and 2-P), and this in turn, after the removal of 1-P, allows the binding of (5-P and 4-P) (Figure 3). This sequentially allowed binding followed by the cleavage of phosphate groups explains the generation of Ins(2,4,6)P_3. Similarly, the sequential bindings and the cleavages of the phosphate groups of (6-P and 1-P), (4-P and 5-P), and then (2-P and 1-P) or (2-P and 3-P) for the generation of Ins(1,3,5)P_3 are well supported by the modeling experiment (data not shown).

Since the enzyme is able to cleave any of the phosphate groups of phytate, it is highly likely to hydrolyze Ins(1,3,5)P_3 and Ins(2,4,6)P_3 further at a rate comparable to that of hydrolyzing InsP_1s. There is no steric limitation in the simulated binding of each of the Ins(1,3,5)P_3 or Ins(2,4,6)P_3 molecules to the active site. However, under a test tube condition in which produced phosphate is not removed, further degradation of the InsP_3s should be very slow, not only due to the reduced turn-over rate for the hydrolysis of nonadjacent phosphate groups, but also due to the increased susceptibility of the enzyme to the product inhibition (Figure 5b). In a physiological situation, the less-phosphorylated *myo*-inositols could be further degraded by the enzyme, owing to the utilization of the produced phosphate ions.

Biological Implications

Phytate is responsible for storing more than 80% of the total phosphorus in cereals and legumes. Since monogastric animals such as pigs, poultry, and fish are not able to metabolize phytate, phytase is normally added in animal feed to reduce phosphorus excretion. The thermostability of TS-Phy is a highly desirable property considering the high temperature employed in processing animal feed. The catalytic property of this valuable enzyme has been poorly characterized. Furthermore, since the enzyme is the first example of a β propeller phosphatase, delineating the enzyme mechanism is of great importance. Our proposed mechanism of direct phosphotransfer to the hydroxide bridging two calcium ions is in contrast to the hydrolysis mechanism of many phosphatases belonging to the low or high molecular weight acid phosphatase family, which form a covalent phospho-enzyme intermediate. Instead, it is analogous to the enzyme mechanisms of other bimetal-containing phosphatases, except for the *E. coli* alkaline phosphatase, which lacks a water molecule bridging the bi-Zn center and forms a phospho-enzyme intermediate. The number of metal ions at the active site of TS-Phy, which is four, is unusual among metal-containing phosphatases. The clustered calcium ions could allow for efficient binding of two phosphate groups of a substrate simultaneously and could effectively stabilize the transition-state intermediate, while two of them (Ca5 and Ca6) play the role of increasing the nucleophilicity of the bridging water molecule.

The existence of the two nonequivalent phosphate binding sites at the relatively narrow active site and the bulky nature of phytate appear to allow binding of only two pairs of adjacent phosphate groups of phytate. Sequential cleavages and bindings of the phosphate groups of the intermediates lead to the formation of the alternately dephosphorylated InsP_3s, and the process is likely to continue until all the phosphomonoester bonds of phytate are cleaved off under physiological conditions. The complete hydrolysis of phytate by the enzyme, which we propose on the basis of its capability to cleave any phosphate group of phytate, is another highly desired property for the biotechnological application of the enzyme.

Experimental Procedures

Data Collection and Structure Determination

Overexpression in *Bacillus subtilis* and purification of the enzyme were described [27]. The crystals of TS-Phy in complex with phosphate were obtained by cocrystallization in the presence of 4 mM $CaCl_2$ and 4 mM sodium phosphate in the precipitant solution containing 20% 2-methyl-2,4-pentanediol, 0.1 M 2-morpholinoethanesulfonic acid (pH 6.5). The diffraction data were measured on a DIP2020 area detector, with a graphite-monochromated Cu$K\alpha$ X-ray generated by a MacScience M18XHF rotating anode generator operated at 90 mA and 50 kV at room temperature. The crystals belong to the space group $P2_12_12_1$ with unit cell dimensions of a = 50.378, b = 65.644, and c = 104.767 Å. One molecule of TS-Phy is contained in the asymmetric unit. The structure of the complex was determined by direct refinement of the structure of TS-Phy [17] against the diffraction data using CNS [28] with the refitting of the side chains near the bound phosphate ions. The statistics for the final structures are shown in Table 1.

Measurement of Enzymatic Activity

Phytase activities of the wild-type and the mutant enzymes were assayed by measuring the liberation of orthophosphate using the modified method of Engelen et al. [29], which uses molybdovanadate as a coloring reagent. The enzymatic reaction was started by the addition of 100 μl enzyme solution to 400 μl assay mixture, containing 2 mM sodium phytate, 2 mM $CaCl_2$, and 0.1 M Tris-HCl (pH 7.0). The reaction mixture was incubated at 37°C for 30 min, and the reaction was stopped by adding 500 μl coloring reagent solution containing 2.5% ammonium heptamolybdate, 0.175% ammonia, 0.1425% ammonium vanadate, and 22.75% nitric acid. Any cloudiness was removed by centrifugation prior to the absorbance measurement at 415 nm.

Measurement of Kinetic Constants for Ins(2)P_1

To determine kinetic constants of the enzymatic dephosphorylation of Ins(2)P_1, 50 μl TS-Phy (0.19 mg/ml in 100 mM Tris-HCl [pH 7.0]) was added to sequentially diluted solutions of the Ins(2)P_1 (0.5–19 mM) and incubated at 37°C. Each of the enzymes and Ins(2)P_1 was preincubated with 2 mM $CaCl_2$ at 4°C over 12 hr. At several time points, the liberated inorganic phosphate was quantified as described above. A double reciprocal plot of the initial reaction velocities and the concentrations of Ins(2)P_1 was used to deduce K_M, k_{cat}, and V_{max}.

Analysis of the Inhibition by Fluoride Ion

Spectrofluorometric assays of TS-Phy activity were carried out in a reaction buffer containing phytate, NaF, and $CaCl_2$. After brief mixing in a tube, the reaction mixture was incubated at 37°C. Initial velocities were determined using initial data points showing a linear increase in the production of inorganic phosphate. No curvature in the initial part of the progress curves of the hydrolysis of phytate indicated that a steady state was attained before the measurements. Apparent K_i value of F^- against TS-Phy was determined from a double reciprocal plot of the reaction velocities and concentrations of phytate.

Acknowledgments

We gratefully acknowledge the use of the X-ray Facility at Pohang Light Source (Pohang, Korea) for the data collection. This work was supported by the Creative Research Initiatives of the Korean Ministry of Science and Technology and by the Technology Development Program for Agriculture and Forestry, Ministry of Agriculture and Forestry, Republic of Korea and by a grant from the Brain Korea 21 Project to S.S.

Received: May 9, 2001
Revised: June 25, 2001
Accepted: August 7, 2001

References

1. Vincent, J.B., Crowder, M.W., and Averill, B.A. (1992). Hydrolysis of phosphate monoesters: a biological problem with multiple chemical solutions. Trends Biochem. Sci. *17*, 105–110.
2. Coleman, J.E. (1992). Structure and mechanism of alkaline phosphatase. Annu. Rev. Biophys. Biomol. Struct. *21*, 441–483.
3. Jones, S.R., Kindman, L.A., and Knowles, J.R. (1978). Stereochemistry of phosphoryl group transfer using a chiral [16O, 17O, 18O] stereochemical course of alkaline phosphatase. Nature *275*, 564–565.
4. Kim, E.E., and Wyckoff, H.W. (1991). Reaction mechanism of alkaline phosphatase based on crystal structures. Two-metal ion catalysis. J. Mol. Biol. *218*, 449–464.
5. Zhang, Z.Y. (1998). Protein-tyrosine phosphatases: biological function, structural characteristics, and mechanism of catalysis. Crit. Rev. Biochem. Mol. Biol. *33*, 1–52.
6. Pannifer, A.D., Flint, A.J., Tonks, N.K., and Barford, D. (1998). Visualization of the cysteinyl-phosphate intermediate of a protein-tyrosine phosphatase by X-ray crystallography. J. Biol. Chem. *273*, 10454–10462.
7. Ostanin, K., Harms, E.H., Stevis, P.E., Kuciel, R., Zhou, M.M., and Van Etten, R.L. (1992). Overexpression, site-directed mutagenesis, and mechanism of *Escherichia coli* acid phosphatase. *J. Biol. Chem. 267*, 22830–22836.
8. Lindqvist, Y., Schneider, G., and Vihko, P. (1994). Crystal structures of rat acid phosphatase complexed with the transition-state analogs vanadate and molybdate. Implications for the reaction mechanism. Eur. J. Biochem. *221*, 139–142.
9. Porvari, K.S., et al., and Vihko, P.T. (1994). Site-directed mutagenesis of prostatic acid phosphatase. Catalytically important aspartic acid *258*, substrate specificity, and oligomerization. J. Biol. Chem. *269*, 22642–22646.
10. Wynne, C.J., Hamilton, S.E., Dionysius, D.A., Beck, J.L., and de Jersey, J. (1995). Studies on the catalytic mechanism of pig purple acid phosphatase. Arch. Biochem. Biophys. *319*, 133–141.
11. Barford, D., Das, A.K., and Egloff, M.P. (1998). The structure and mechanism of protein phosphatases: insights into catalysis and regulation. Annu. Rev. Biophys. Biomol. Struct. *27*, 133–164.
12. Ullah, A.H., and Dischinger, H.C., Jr. (1993). *Aspergillus ficuum* phytase: complete primary structure elucidation by chemical sequencing. Biochem. Biophys. Res. Commun. *192*, 747–753.
13. Ullah, A.H., and Sethumadhavan, K. (1998). Differences in the active site environment of *Aspergillus ficuum* phytases. Biochem. Biophys. Res. Commun. *243*, 458–462.
14. Lim, D., Golovan, S., Forsberg, C.W., and Jia, Z. (2000). Crystal structures of *Escherichia coli* phytase and its complex with phytate. Nat. Struct. Biol. *7*, 108–113.
15. McTigue, J.J., and Van Etten, R.L. (1978). An essential arginine residue in human prostatic acid phosphatase. Biochim. Biophys. Acta *523*, 407–421.
16. Van Etten, R.L. (1982). Human prostatic acid phosphatase: a histidine phosphatase. Ann. NY Acad. Sci. *390*, 27–51.
17. Ha, N.C., et al., and Oh, B.H. (2000). Crystal structures of a novel, thermostable phytase in partially and fully calcium-loaded states. Nat. Struct. Biol. *7*, 147–153.
18. Oubrie, A., Rozeboom, H.J., Kalk, K.H., Duine, J.A., and Dijkstra, B.W. (1999). The 1.7 Å crystal structure of the apo form of the soluble quinoprotein glucose dehydrogenase from acnetobacter calcoaceticus reveals a novel internal conserved sequence repeat. J. Mol. Biol. *289*, 319–333.
19. Faber, H.R., Groom, C.R., Baker, H.M., Morgan, W.T., Smith, A., and Baker, E.N. (1995). 1.8 Å crystal structure of the C-terminal domain of rabbit serum haemopexin. Structure *3*, 551–559.
20. Fülöp, V., and Jones, D.T. (1999). β propellers: structural rigidity and functional diversity. Curr. Opin. Struct. Biol. *9*, 715–721.
21. Holm, L., and Sanders, C. (1993). Dali: a network tool for protein structure comparison. Trends Biochem. Sci. *20*, 478–480.
22. Wyss, M., et al., and van Loon, A.P.G.M. (1999). Biochemical characterization of fungal phytases (myo-inositol hexakisphosphate phosphohydrolases): catalytic properties. Appl. Environ. Microbiol. *65*, 367–373.
23. Basolo, F., and Pearson, R.G. (1967). Acid-Base Properties of Complex Ions in Mechanisms of Inorganic Reactions (New York: Wiley).
24. Oh, B.C., et al., and Oh, T.K. (2001). Calcium dependent catalytic activity of a novel phytate from *Bacillus amyloliquefaciens* DS11. Biochemistry, *40*, 9669–9676.
25. Heikinheimo, P., et al., and Goldman, A. (2001). Toward a quantum-mechanical description of metal-assisted phosphoryl transfer in pyrophosphatase. Proc. Natl. Acad. Sci. USA *98*, 3121–3126.
26. Kerovuo, J., Rouvinen, J., and Hatzack, F. (2000). Analysis of myo-inositol hexakisphosphate hydrolysis by *Bacillus* phytase: indication of a novel reaction mechanism. Biochem. J. *352*, 623–628.
27. Ha, N.C., Kim, Y.O., Oh, T.K., and Oh, B.H. (1999). Preliminary X-ray crystallographic analysis of a novel phytase from a *Bacillus amyloliquefaciens* strain. Acta Crystallogr. D *55*, 691–693.
28. Brünger, A.T., et al., and Warren, G.L. (1998). Crystallography & NMR system: a new software suite for macromolecular structure determination. Acta Crystallogr. D *54*, 905–921.
29. Engelen, A.J., van der Heeft, F.C., Randsdorp, P.H., and Smit, E.L. (1994). Simple and rapid determination of phytase activity. J. AOAC Int. *77*, 760–764.
30. Esnouf, R.M. (1997). An extensively modified version of MolScript that includes greatly enhanced coloring capabilities. J. Mol. Graph. Model. *15*, 132–134.
31. Jones, T.A., and Kjeldgaard, M. (1993). O version 5.9. (Uppsala, Sweden: Uppsala University).

Accession Numbers

The atomic coordinates have been deposited in the Protein Data Bank with the accession code 1H6L.